The Magneto-Optical Response of Diluted Magnetic Semiconductor CdTe–$Cd_{1-x}Mn_xTe$ Multi Quantum Wells in the Voigt Configuration

M. Hidari and S. Farjami Shayesteh*

Department of Physics, University of Guilan, P.O. Box. 1914, Rasht, Iran

(Received June 1, 2009; in final form June 9, 2009)

We have calculated the *s*- and *p*-polarized far infrared magnetoplasmon spectra of doped CdTe–$Cd_{1-x}Mn_xTe$ multi quantum wells in the presence of a static magnetic field up to 20 T parallel to the surface of the layers using a macroscopic model based on effective medium theory, using a novel approach which gives a good account of the data together with a clear physical interpretation of the various spectral features, such as the free carrier and optical phonon properties. The results show that the transverse optical modes (for the whole composition range, $x = 0$ to 1) are sensitive and change linearly with respect to the composition parameter. In *p*-polarized reflectivity the cyclotron resonance experiences a blue shift when the magnetic field strength increases. Also, the analysis of the dielectric tensor function and the Voigt dielectric function is used to determine the carriers' cyclotron effective masses (for both holes and electrons) as a function of composition. Furthermore, a modified random element iso-displacement approach has been extended for the multi layers to analyze the influence of the composition on the optical phonon response in the barrier layer.

PACS numbers: 78.30.Fs, 78.30.−j, 78.20.Ls, 73.21.Fg

1. Introduction

Recent progress in growth techniques, such as metalorganic vapour-phase epitaxy (MOVPE) and molecular beam epitaxy (MBE), makes it possible to study optical properties of CdTe–$Cd_{1-x}Mn_xTe$ multi quantum well (MQW). Dilute magnetic semiconductors (DMS) CdTe–$Cd_{1-x}Mn_xTe$ have attracted much attention both from a fundamental physics point of view as well as for novel device applications [1, 2] because of their giant and tuneable spin-splitting which is of great importance for spintronics. This structure has provided us with an ideal system to study these interesting physical properties.

The effective medium approach has been applied for analysis of experimental results on doped semiconductor MQW, so that the infrared response was due to free carriers (plasma response) as well as optical phonons. There should be advantage in extending work of this kind by inclusion of an applied magnetic field so that dielectric tensor takes a magnetoplasma form. In order to get the complete form of dielectric tensor in the infrared in general we include both optical phonon and magnetoplasma terms. The effect of the external magnetostatic fields on the optical response in MQWs has been the subject of active research during the last decade. According to the direction of the applied magnetic field three configurations are defined: the perpendicular [3, 4], Faraday [5, 6] and Voigt [7, 8] configurations.

The effective masses of the carriers (electrons and holes) are the basic parameters for semiconductor MQWs. However, only limited data have been reported so far for the II–VI family of MQWs [9]. In doped samples there exist the longitudinal optical phonon–plasmon coupled (LPP) modes, which are interesting for physical interactions between the lattice vibration and free carriers, and can be directly investigated using infrared magnetoplasmon reflectivity spectra. Cyclotron resonance is an excellent method for obtaining the effective mass of carriers.

By changing the ratio of Mn in the barriers ($Cd_{1-x}Mn_xTe$) it is possible to tune the magnetic properties. This material seems to be very useful for use as the barrier material in spintronic devices. The lattice dynamics of bulk $Cd_{1-x}Mn_xTe$ has been investigated in detail, both experimentally and theoretically in the absence of external magnetic field [10]. In the previous work, we present magneto-optical properties of doped $Cd_{1-x}Mn_xTe$ alloy [11]. However, despite progress in device performance, understanding of optical and structural properties of the doped CdTe–$Cd_xMn_{1-x}Te$ MQWs is still not satisfactory.

The purpose of this work to investigate the phonon and free carrier properties of semi-magnetic CdTe–$Cd_{1-x}Mn_xTe$ multi quantum wells by far infrared magneto-reflectivity as a function of composition, x, and applied magnetic field, B. Calculations have been carried out for the Voigt configuration (the magnetic field parallel to the surface and perpendicular to the direction of the propagation). Also, we calculated the optical

* corresponding author; e-mail: saber@guilan.ac.ir

phonon frequencies by using a modified random element iso-displacement (MREI) model [11] which we extended for the doped multilayer structure.

2. Magnetoplasmon dielectric tensor of MQWs

One of the main parameters needed for optoelectronics device design is the interaction of free carriers with photon in the low frequency region. The detailed and accurate knowledge of the dielectric function is necessary to evaluate the optical absorption of materials. In the far infrared, optical propagation frequency occurs in the long wavelength regime $\lambda \gg d$, where λ is the optical wavelength and d the MQW period. In this case it might be expected that the equation for optical propagation reduced to those for a bulk uniaxial medium [12], since the macroscopic symmetry of the MQW is uniaxial with uniaxis normal to the layers. In general, the dielectric tensor characterise the response of a medium to electromagnetic waves. The influence of the elementary excitation (plasmon and optical phonon), can be included by means of an appropriate contribution to the dielectric tensor. A schematic drawing of the Voigt configuration and the coordinate axes used for the calculations for MQWs made up of two alternating semiconductor layers is shown in Fig. 1. For CdTe–$Cd_xMn_{1-x}Te$ MQWs with

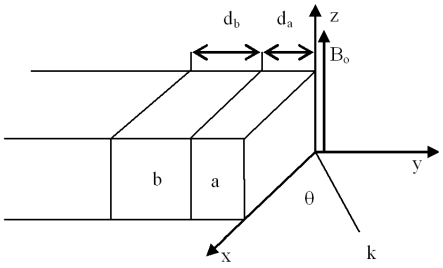

Fig. 1. Schematic diagram of the Voigt configuration and the coordinate axes used for the calculations. x–z plane is parallel to MQWs interfaces, external magnetic field B_0 is applied along the z-axis and incidence light wave vector k is parallel to x–y plane.

a two-component magnetoplasma, i.e. electrons and holes and optical phonons, the frequency-dependent dielectric tensor is anisotropic and given by [13–15]:

$$\begin{bmatrix} \varepsilon_1 & -\mathrm{i}\varepsilon_T & 0 \\ \mathrm{i}\varepsilon_T & \varepsilon_2 & 0 \\ 0 & 0 & \varepsilon_3 \end{bmatrix} \tag{1}$$

with elements,

$$\varepsilon_1 = f_a\varepsilon_1^a + f_b\varepsilon_1^b - f_a f_b \frac{\left(\varepsilon_T^a - \varepsilon_T^b\right)^2}{f_a\varepsilon_1^b + f_b\varepsilon_1^a}, \tag{2}$$

$$\varepsilon_2 = \frac{\varepsilon_1^a\varepsilon_1^b}{f_a\varepsilon_1^b + f_b\varepsilon_1^a}, \tag{3}$$

$$\varepsilon_3 = f_a\varepsilon_3^a + f_b\varepsilon_3^b \tag{4}$$

and

$$\varepsilon_T = \frac{f_a\varepsilon_T^a\varepsilon_1^b + f_b\varepsilon_T^b\varepsilon_1^a}{f_a\varepsilon_1^b + f_b\varepsilon_1^a}, \tag{5}$$

where $f_a = \frac{d_a}{d_a+d_b}$ and $f_b = \frac{d_b}{d_a+d_b}$ are the volume fractions occupied by layer a and b. We take the basic components in the forms

$$\varepsilon_1^\alpha = \varepsilon_\infty^\alpha \left\{ 1 + \sum_j \frac{\omega_{\mathrm{LO}j}^2 - \omega_{TOj}^2}{\omega_{TOj}^2 - \omega^2 - \mathrm{i}\omega\Gamma_{TOj}} + \sum_\mu \frac{\left(\omega_{p\mu}^\alpha\right)^2 \left(\omega + \mathrm{i}\Gamma_{c\mu}^\alpha\right)}{\omega\left[\left(\omega_{c\mu}^\alpha\right)^2 - \left(\omega + \mathrm{i}\Gamma_{c\mu}^\alpha\right)^2\right]} \right\}, \tag{6}$$

$$\varepsilon_3^\alpha = \varepsilon_\infty^\alpha \left[1 + \sum_j \frac{\omega_{\mathrm{LO}j}^2 - \omega_{TOj}^2}{\omega_{TOj}^2 - \omega^2 - \mathrm{i}\omega\Gamma_{TOj}} + \sum_\mu \frac{(\omega_{p\mu}^\alpha)^2}{\omega^2 - \mathrm{i}\omega\Gamma_{p\mu}^\alpha} \right], \tag{7}$$

$$\varepsilon_T^\alpha = \sum_\mu \frac{\varepsilon_\infty^\alpha (\omega_{p\mu}^\alpha)^2 \omega_{c\mu}^\alpha}{\omega\left[\left(\omega_{c\mu}^\alpha\right)^2 - \left(\omega + \mathrm{i}\Gamma_{c\mu}^\alpha\right)^2\right]}, \tag{8}$$

where ω_{Tj} is the TO phonon frequency, Γ_{Tj} is the phonon damping parameter and S_j is the oscillator strength. The plasma frequency of free carriers for layer α (a or b) is defined as:

$$\omega_{p\mu}^\alpha = \left(\frac{N_\mu^\alpha e^2}{\varepsilon_\infty^\alpha m_\mu^{*\alpha}} \right)^{1/2} \tag{9}$$

and the cyclotron frequency for layer α (a or b) is defined by:

$$\omega_{C\mu}^\alpha = \frac{eB_0}{m_\mu^{*\alpha}}, \tag{10}$$

where $\varepsilon_\infty^\alpha$ the background dielectric constant, N_μ^α is the carrier concentration and $m_\mu^{*\alpha}$ is the cyclotron effective mass for carrier μ (e or h).

The Voigt dielectric function depends on the cyclotron frequency and is given by

$$\varepsilon_{\mathrm{V}} = \frac{\varepsilon_1\varepsilon_2 - \varepsilon_T^2}{\varepsilon_2}, \tag{11}$$

which gives the general behaviour of p-polarized reflectivity and for MQW is given by

$$\langle\varepsilon_{\mathrm{V}}\rangle = f_a\varepsilon_{\mathrm{V}}^a + f_b\varepsilon_{\mathrm{V}}^b. \tag{12}$$

3. Results and discussion

In this section we present the numerical investigation of the optical and electronic properties of CdTe–$Cd_{1-x}Mn_xTe$ MQWs. For our study we used MQW samples which contain 200 periods with nominal CdTe well width 10 nm and $Cd_{1-x}Mn_xTe$ barrier width 20 nm with manganese concentration in the range $0 < x < 1$, and the carrier concentrations are $n_{\mathrm{e}} = 2 \times 10^{12}$ cm^{-2} and $n_{\mathrm{h}} = 1 \times 10^9$ cm^{-2}.

For the numerical calculations, the phonon frequencies are calculated using an MREI model [11, 16] which we extended for the doped multilayer structure.

The dependence of the effective masses of electrons and holes in the CdTe–$Cd_{1-x}Mn_xTe$ MQWs are given respectively by [17, 18]:

$$m_e^* = (0.11 + 0.067x)m_0, \quad (13)$$

$$m_h^* = (0.60 + 0.21x + 0.15x^2)m_0. \quad (14)$$

There exist many parameters which affect on the effective mass of carriers in the CdTe–$Cd_{1-x}Mn_xTe$ MQWs, such as growth direction, well width, strain, polaron effect due to the electron–phonon interaction [19, 20]. Equations (13) and (14) give only the dependence of the effective mass to composition and the effect of the other parameters is ignored. Parameters used to model the far infrared magnetoplasma reflectivity at room temperature are presented in Table.

TABLE

Parameters used to model the far infrared magnetoplasma reflectivity at room temperature.

Composition x	m^*_{hh}/m_0 [17]	m^*_e/m_0 [17]	ω_{LO} [cm^{-1}] MnTe-like [our result, 11]	ω_{TO} [cm^{-1}] MnTe-like [our result, 11]	ω_{LO} [cm^{-1}] CdTe-like [our result, 11]	ω_{TO} [cm^{-1}] CdTe-like [our result, 11]
0.20	0.648	0.123	207.50	182.50	146.00	142.00
0.40	0.708	0.136	205.10	185.00	150.10	141.40
0.60	0.780	0.1502	200.50	186.50	155.15	140.90
0.80	0.864	0.161	197.50	199.50	159.00	140.00

The analysis uses the s (electric field $\boldsymbol{E}$ parallel to external magnetic field B_0)- and p (magnetic field $\boldsymbol{H}$ parallel to B_0)-polarized far infrared oblique incidence reflectivity in the Voigt configuration by considering the interaction of infrared radiation with MQWs, by using a transfer matrix method. In long wavelength limit, the optical properties of MQWs are satisfactorily described by an effective medium bulk slab model modified to take account of the effect of the quasi-two-dimensional behaviour on the plasmon in the wells.

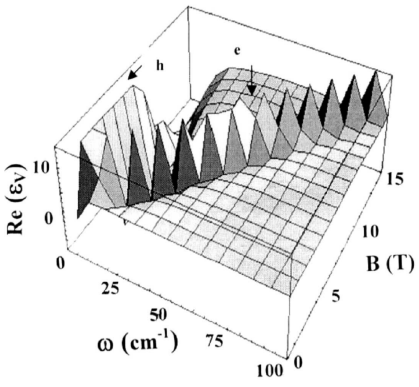

Fig. 2. The Voigt dielectric function as a function of magnetic field, B, and ω (cm^{-1}) for composition $x = 0.4$, without the phonon response. The cyclotron resonances for holes and electrons are marked with arrows.

In Fig. 2 we plot the frequency dependence of the real part of the Voigt dielectric tensor as a function of wave number and magnetic field for a two-component magnetoplasma (electrons and holes) in doped CdTe–$Cd_{1-x}Mn_xTe$ MQWs from which the effects of the optical phonons were excluded. The features in Fig. 2 marked by arrows come from the cyclotron resonance of holes (h) and electrons (e) respectively. The frequencies of all magnetoplasma cyclotron resonance (both electron and hole) features and the positions of zeros in ε_V are directly related to the carrier effective masses and are functions of the applied magnetic field. Figure 3 shows the variation of the real part of the Voigt tensor as a function of ω and B for $x = 0.8$ when the optical phonon response is included in the dielectric tensor.

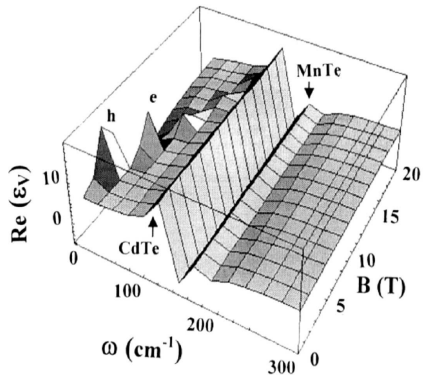

Fig. 3. The variation of the real part of the Voigt dielectric function of CdTe–$Cd_{1-x}Mn_xTe$ MQW with ω and B for $x = 0.8$. The arrows indicate the CdTe-like and MnTe-like sublattice responses.

As shown in Fig. 3 the positions of the optical phonon features are (as indicated by arrows) independent of the

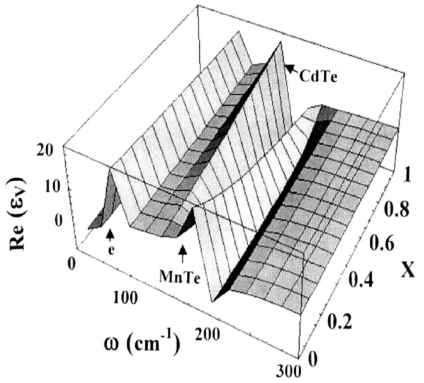

Fig. 4. The Voigt dielectric function of DMS CdTe–$Cd_{1-x}Mn_xTe$ MQW with $B = 10$ T as a function of ω and composition, x. The arrows indicate the CdTe-like and MnTe-like sublattice responses. The dashed arrow marks the electron cyclotron resonance.

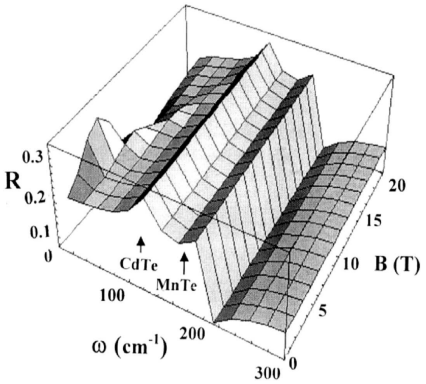

Fig. 6. p-polarized magnetoplasmon reflectivity of a sample with $x = 0.4$ as a function of magnetic field B, in the Voigt configuration. The arrows indicate the CdTe--like and MnTe-like sublattice responses.

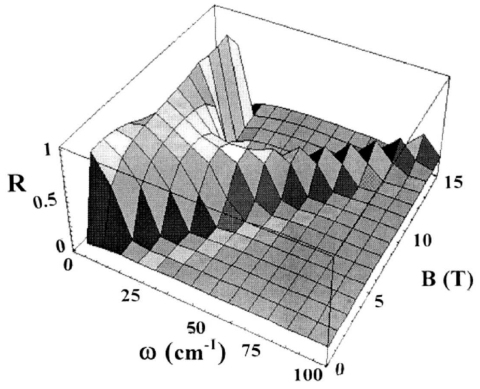

Fig. 5. p-polarized magnetoplasmon reflectivity of a sample with $x = 0.4$ as a function of magnetic field B, in the Voigt configuration without any phonon response.

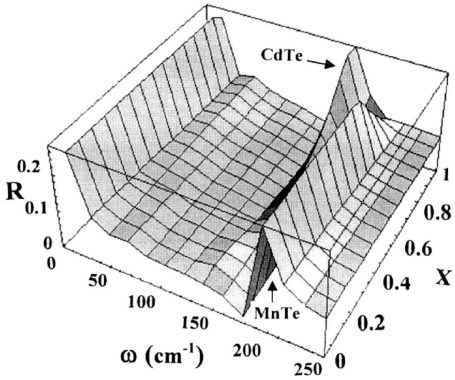

Fig. 7. p-polarized magnetoplasmon reflectivity of CdTe–$Cd_{1-x}Mn_xTe$ MQW as a function of ω and x for $B = 10$ T.

magnetic field. The real part of the Voigt dielectric function as a function of composition, x, and frequency, ω, is illustrated in Fig. 4 for $B = 10$ T, in which the magnetoplasmon and the phonon term have been included in the analysis of the calculated data. The oscillator strength of the sample shows composition dependence and the positions of the CdTe-like and MnTe-like modes are shifted (Fig. 4). According to the theoretical MREI calculation the $Cd_{1-x}Mn_xTe$ barrier layer should exhibit two-mode behavior [11]. The p-polarized 45° oblique incidence power reflectivity spectra are presented in Fig. 5 for doped CdTe–$Cd_{0.6}Mn_{0.4}Te$ MQW for several magnetic fields up to 20 T, in which we have omitted any contribution from optical phonons.

All resonances in the Voigt permittivity (Fig. 4) show up as quite strong features in the p-polarized reflectivity (Figs. 5 and 6). The barrier layers ($Cd_{1-x}Mn_xTe$) show two-mode phonon behaviour in the spectral range from about 140 to 210 cm^{-1}. The transverse optical CdTe--like and MnTe-like sublattice phonon modes are at wave numbers of about 141.40 and 185.00 cm^{-1}, respectively. The reststrahlen band of the CdTe (well layers) is located between the TO (141 cm^{-1}) and the plasma shifted LO (167 cm^{-1}) frequencies. The p-polarized magnetoplasmon reflectivity experiences a blue shift when the magnetic field strength increases (below 110 cm^{-1}). In high magnetic fields the electron cyclotron frequency occurs in the CdTe-sublattice frequency region, so that the magnetoplasma features will mix with and be shifted by the optical phonon modes. Let us note the sharp resonance near the $\omega_{LO} = 210$ cm^{-1} (MnTe-like) mode due to absorption of p-polarized light which is well known as the Berreman effect [21]. In Fig. 7 the CdTe-like and MnTe--like ω_{TO} frequencies shift gradually with variation of composition, x.

In Fig. 8, we compare the magneto-optical response of the p- and s-polarized reflectivity. All features in the s-polarization spectrum (Fig. 8b) are independent of the magnetic field as expected because the s-polarization reflection is dependent on the dielectric component ε_3 (Eqs. (7)) which is independent of the electron and hole

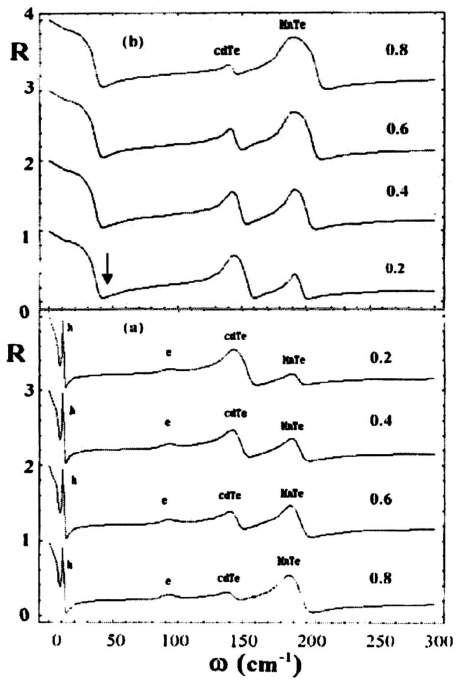

Fig. 8. Comparison of (a) p and (b) s-polarization magnetoplasmon reflectivity of CdTe–$Cd_{1-x}Mn_xTe$ MQW for different compositions $x = 0.8$, 0.6, 0.4, 0.2 at $B = 10$ T.

cyclotron resonances. The feature in s-polarization reflectivity marked by an arrow was assigned to the plasma response (below 80 cm^{-1}). In polar semiconductors, plasmon of free carriers intract with longitudinal optical (LO) phonon via macroscopic electric field. Due to the effect of the LO phonon–plasmon coupling (polaronic effects) the frequencies of the LO phonons are shifted [9, 22] and allow the determination of the free carrier concentration and it is the only significant effect of the plasmon on the phonon response. The experimental results have shown that the polaronic effects on the effective mass of MQWs are reduced in comparison with the results for the bulk semiconductor [9].

Dramatic changes in the band structure and lattice parameters result from a change in the Mn composition in the barrier layers. The oscillator strength of the MnTe sublattice resonance increases with increasing Mn composition and this can be used to monitor the composition rate.

4. Conclusion

We have used the far infrared polarized magnetoplasmon reflectivity in the Voigt configuration as a novel approach for the non-destructive optical characterization of the free carriers' cyclotron masses, carrier concentrations and optical phonon properties of CdTe–$Cd_{1-x}Mn_xTe$ MQWs as a function of Mn concentration. The effective medium approach and magnetoplasmon dielectric tensor in which we include both optical phonon and magnetoplasma terms are employed for the analysis of the polarized reflectivity data. An MREI model that we extended for doped multilayer samples has been used to calculate the optical phonon frequencies of CdTe–$Cd_{1-x}Mn_xTe$ MQW: $Cd_{1-x}Mn_xTe$ exhibits 2-mode phonon behaviour, with the phonon modes sensitive to composition. The MnTe-like TO phonon frequency is sensitive to the Mn fraction and shows a blue shift with increasing Mn concentration in the barrier ($Cd_{1-x}Mn_xTe$) layers. Also due to the polaronic effect (plasmon–LO phonon coupling) the frequency of the LO phonon plasma shifted MnTe-like mode is sensitive to the free carrier concentration. Furthermore, the effective cyclotron mass of both species of carriers as a function of Mn concentration can be measured by using the plasmon and cyclotron resonance frequencies. In addition, it is important to provide an accurate description of the vibrational properties because they play a significant role in determining some material properties such as the inter-atomic forces and electron–phonon interactions.

Acknowledgments

The authors would like to thank Prof. T.J. Parker for helpful comments and a critical reading of the manuscript. Also, the authors are thankful to University of Guilan for providing financial support.

References

[1] M. Jain, *Diluted Magnetic Semiconductors*, World Sci., Singapore 1991.

[2] V.F. Aguekian, T. Konatsue, N. Miura, K. Uchida, D. Ashenford, *J. Lumin.* **87**, 506 (2000).

[3] G. Martinez, J.H.J. Escobar, P.H. Hormandez, *Phys. Rev. B* **59**, 1043 (1999).

[4] M.S. Kushawha, *Surf. Sci.* **262**, 451 (1991).

[5] G. Mardinez, P.H. Hermandez, R. Garcia-Sarrano, X.I. Saldana, *Superlattices Microstruct.* **32**, 110 (2002).

[6] M.S. Kushawha, B. Djafari-Rouhani, *Surf. Sci.* **266**, 457 (1992).

[7] J.H. Jacobo-Escobar, *Superlattices Microstruct.* **33**, 145 (2003).

[8] S. Farjami Shayesteh, *Int. J. Infrared Millimeter Waves* **24**, 187 (2003).

[9] A.A. Dremin, D.R. Yakovlev, A.A. Sirenko, S.I. Gubarev, O.P. Sabelsky, A. Wang, M. Bayer, *Phys. Rev. B* **72**, 195337.I (2005).

[10] D.L. Peterson, A. Petrou, A.K. Ramdas, S. Rodreguez, *Phys. Rev. B* **33**, 1160 (1986).

[11] S. Farjami Shayesteh, M. Hidari, *Phys. Status Solidi B* **244**, 2159 (2007).

[12] N. Raj, D.R. Tilley, *Solid State Commun.* **55**, 373 (1985).

[13] F.G. Elmzughi, N.C. Constantinou, D.R. Tilley, *J. Phys., Condens. Matter* **7**, 315 (1995).

[14] S. Kushwaha Manvier, *Surf. Sci. Rep.* **41**, 1 (2001).

[15] E.L. Albuquerque, P. Fulco, *Z. Phys. B* **100**, 263 (1996).

[16] D.N. Talwar, Kito Holliday, *Physica B* **263-264**, 540 (1999).

[17] P. Harrison, *Quantum Wells, Wires and Dots*, Wiley, UK 2000.

[18] F. Long, P. Harison, W.E. Hagston, *J. Appl. Phys.* **79**, 6939 (1996).

[19] A.A. Dremin, D.R. Yakovlev, A.A. Sirenko, S.I. Gubarev, O.P. Shabelsky, A. Waag, M. Bayer, *Phys. Rev. B* **72**, 195337 (2005).

[20] Fei Long, W.E. Hagston, P. Harrison, T. Stirner, *J. Appl. Phys.* **82**, 3414 (1997).

[21] D.W. Berreman, *Phys. Rev.* **130**, 2193 (1963).

[22] T. Dumelow, D.R. Tilley, *J. Opt. Soc. Am. A* **10**, 633 (1993).